Available online at www.sciencedirect.com
SCIENCE DIRECT®
International Journal of Multiphase Flow 30 (2004) 1235–1257
International Journal of Multiphase Flow
www.elsevier.com/locate/ijmulflow

On preferential diffusion of binary component liquid droplets evaporating in a two-phase mixing layer

Kishore K. Varanasi [a], Herek L. Clack [b], Richard S. Miller [a,*]

[a] *Department of Mechanical Engineering, Clemson University, Clemson, SC 29634-0921, USA*
[b] *Department of Mechanical, Materials and Aerospace Engineering, Illinois Institute of Technology, Chicago, IL 60616-3793, USA*

Received 22 September 2003; received in revised form 19 June 2004

Abstract

Numerical simulations of a two-phase binary component droplet laden temporally developing mixing layer are conducted in order to investigate the influence of preferential diffusion of liquid species. A multi-component evaporation model based on classical rapid mixing vaporization and Raoult's law is applied to the Lagrangian description for individual droplets. Results are first presented for single isolated binary component droplets under the same conditions used in the final mixing layer simulations in order to illustrate the models behavior and ability to account for preferential vaporization of the more volatile species. Single droplet simulations are performed for a variety of binary component species pairs having varying properties; including heptane, decane, hexane, hexane–trichloroacetane (TCA), and water. The results illustrate the importance of the latent heat of vaporization, in addition to the traditionally cited boiling temperature, in determining the correct relative volatilities of the liquid species. The results illustrate that species can exhibit strong preferential diffusion effects even with equal boiling temperatures when their latent heats vary substantially. A Lagrangian droplet model is then coupled with the compressible form of the continuity, momentum, energy and species transport equations governing the carrier gas phase. High resolution simulations are conducted of a two-dimensional temporally developing mixing layer with one stream laden with binary component evaporating droplets. Preferential vaporization is found to significantly affect the evaporated species concentrations and distributions within the mixing layer. Evaporative flow saturation is observed, wherein the laden stream becomes saturated before the evaporation is complete. Resulting species concentration distributions within the mixing layer are determined by the coupled effects of

* Corresponding author. Tel.: +1 864 656 6248; fax: +1 864 656 4435.
E-mail address: rm@clemson.edu (R.S. Miller).

0301-9322/$ - see front matter
doi:10.1016/j.ijmultiphaseflow.2004.06.004

preferential vaporization of the more volatile species, and by preferential concentration of droplets within the flow.

Keywords: Direct numerical simulation; Droplet; Turbulence; Two-way coupling; Evaporation; Preferential vaporization

1. Introduction

The vaporization of multicomponent droplet laden turbulent flows is a relevant phenomenon in many practical applications such as diesel and aircraft engines. Prediction of droplet evaporation rates and corresponding flow evolutions can be an important factor in combustion modeling, and can be the controlling factor for energy conversion rates. With the advent of modern high speed computers, high fidelity numerical simulations are being increasingly used to study gas-droplet turbulent flows. Although many two-phase evaporating droplet laden Lagrangian–Eulerian flow simulations have been conducted under various flow modeling approaches (Sirignano, 1993; Crowe et al., 1996; Aggarwal and Peng, 1995; Sirignano, 1999), relatively few "high fidelity" simulations of turbulent flows tracking every individual evaporating droplet have been performed. These investigations, often referred to as "direct numerical simulations" (despite the implicit modeling of the dispersed phase and its coupling to the gas phase), have been largely limited to single component droplet laden flows (Mashayek et al., 1997; Mashayek and Jaberi, 1999; Mashayek, 1998a,b; Miller and Bellan, 1999, 2000; Okong'o and Bellan, 2000; Miller, 2001; Khatumria and Miller, 2003). This is due in part to the complex phenomena involved in multicomponent droplet vaporization; many of which depend on the relative volatilities of the pure component species. One recent exception are the mixing layer simulations performed by Le Clercq and Bellan (2002) using a continuous thermodynamics based statistical model representing the multi-species droplet vaporization. Furthermore, it has been shown by Law et al. (1977) and Sirignano and Law (1978) that the evaporation process of the fuel mixture cannot be described correctly by single-component fuel models based on averaged properties as a result of the variations of thermophysical properties and volatilities of the fuel components (discussed below).

A variety of models have been proposed to describe single component, single isolated droplet transport (see above and Miller et al., 1998). The classical evaporation model for a single-component droplet, also referred to as the "D^2 law", was first introduced by Godsave (1953) and Spalding (1953). This model assumes a uniform internal droplet temperature and a quasi-steady state for the gas-phase leading to a logarithmic form for the mass transfer potential. In order to include the effects of transient droplet heating, the evaporation rate is coupled with a time dependent energy equation to obtain the "rapid mixing model" (Aggarawal et al., 1984), which is the most commonly used model for modern spray calculations (e.g. Chen and Pereira (1996)). Bellan and Summerfield (1978) first introduced the non-equilibrium Langmuir–Knudsen evaporation law for a single-component droplet for use in combustion models and found non-equilibrium effects to be important for droplet sizes found in practical spray situations. Miller et al. (1998) recently evaluated eight Lagrangian droplet models from the perspective of both accuracy and computational efficiency. Both the equilibrium and non-equilibrium evaporation models were

evaluated for a single isolated droplet through comparisons with experiments. All models were found to perform nearly identically for low evaporation rates; however, for high evaporation rates in which the carrier gas temperature is larger than the liquid boiling temperature, substantial deviations among the various model predictions were observed. They further found that non-equilibrium effects can become important for relevant initial droplet diameters ($\leqslant 50$ μm) when the evaporation rate is sufficiently large, and therefore suggested a model based on the Langmuir–Knudsen evaporation law combined with an analytical heat transfer correction for vaporization effects.

Multicomponent droplet evaporation is considerably more complex than vaporization of single component fuels. This is due in part to the range of physical processes controlling the relative volatilities of the pure component species (Sirignano, 1993). Wood et al. (1960) identified "batch distillation" due to wide volatility differentials as the main controlling parameter for changing the internal composition of droplets. Landis and Mills (1974) were among the first to identify internal diffusional resistance as another possible controlling process for multicomponent droplet evaporation. In the case of fast vaporization, preferential vaporization may occur since the concentration inside cannot reach the surface quickly enough due to diffusional resistance. However, their analysis does not take into account the effects of circulation inside the drop which would tend to bring the results closer to those of the batch-distillation model. The importance of liquid-phase mass diffusion was also investigated by Randolph et al. (1986), whose experimental results revealed that the effectiveness of mass diffusion decreases with increasing volatility differentials of the mixture; the conclusion was that the gasification mechanism is intermediate between batch distillation and a steady state controlled by diffusion. Lara-Urbaneja and Sirignano (1981) examined the effects of convective transport through internal circulation and found that the internal circulation reduces the characteristic length of diffusion by about one-third, which has the effect of reducing the characteristic diffusion time scale by approximately an order of magnitude.

The purpose of the present paper is to compile a general vaporization model for multicomponent droplet laden flows relevant to high fidelity simulations and to conduct simulations of a temporally developing mixing layer with one droplet laden stream. The starting point for the formulation and approach are the single component droplet laden mixing layer studies of Miller (2001) and Khatumria and Miller (2003) which are based on established Lagrangian droplet model equations validated with experimental data (Miller et al., 1998). For the purposes of the present study, only binary component fuel droplets are addressed; although the model developed is not limited specifically to two components. Species pairs of hexane, decane, heptane, hexane–trichloroacetane (TCA) and water are chosen based on their representative property values. As discussed in what follows the properties of these specific species illustrate the potential importance of the latent heat of vaporization in addition to the traditionally cited boiling temperature (Sangiovanni and Kesten, 1976; Law, 1990; Kim et al., 1990; Kramlich, 1990; Presser et al., 1992) in determining relative species volatilities.

Following Miller (2001) and Khatumria and Miller (2003) the present study is limited to 2D mixing layers as a model flow due to the relatively high computational cost of two-phase 3D simulations. Although lacking the vortex stretching mechanism of small scale turbulence generation, 2D mixing layers nevertheless contain many of the flow features inherent to 3D turbulent flows which relate to the present study, including vortical structures and pairing, preferential concentration, particle-flow interaction, and evaporative flow saturation (Miller, 2001). In addition, limiting

the simulations to 2D allows use of a much higher resolution grid and the consideration of as many as eight initial vortical structures with four pairing events, resulting in a highly convoluted final mixing zone. The study involves the extension of the prior single component droplet equations to include multicomponent species effects, and simulation results for a binary component droplet laden temporally developing mixing layer. In addition, results are first presented for single isolated droplets in quiescent environments having identical thermodynamic parameters as those used in the final mixing layer simulations. These are used to more simply illustrate the behavior of binary component droplet evaporation which will aid in interpreting the final mixing layer simulation results. The paper is organized as follows. The formulation and problem description are presented in Sections 2 and 3, respectively. Results for both single droplets and the mixing layer are provided in Section 4, and conclusions are given in Section 5.

2. Formulation

The governing equations describe the Lagrangian transport of discrete multicomponent evaporating droplets through a continuous, calorically perfect carrier gas flow. Under the present conditions the droplets are assumed to be spherical and much smaller than the undisturbed turbulence flow length scales, to occupy a negligible volume fraction relative to the gas phase, and to have moderate to small droplet Reynolds numbers (negligible wake effects). Droplet momentum transport is considered to be a function of the drag force only (i.e. gravity, Basset history, added mass and other terms are neglected). Each droplet is assumed to have Biot number much less than unity, thus maintaining uniform internal temperature. Thermal energy exchange with the gas phase is assumed to be only through convection/conduction heat transfer (negligible radiation effects). The steady gravitational settling velocity is much smaller than the characteristic flow velocity for all cases considered in this study; therefore, gravity effects are neglected in the droplet formulation. Furthermore, nucleation, coalescence, breakup and collisions of droplets are neglected. Internal droplet flow and diffusional penetration of gas phase species into the drops are neglected. It is also assumed that constant values can be prescribed for the gas-phase viscosity, thermal conductivity and species diffusivity independently of the local mixture fraction. The formulation and approach adopted are multicomponent extensions of models which have appeared before and will therefore only be summarized in what follows. Readers are referred to Miller and Bellan, 1999, 2000; Miller, 2001; Khatumria and Miller, 2003 for additional details.

Under the dilute dispersed phase assumption the equations governing the gas phase flow (carrier gas plus vapor mixture) are the (non-volume fraction corrected) compressible forms of the continuity equation, the Navier–Stokes equations, the energy equation, and species conservation equations for the carrier gas and each of the binary component vapor phases; augmented by phase coupling terms described below. The ideal gas law is employed for the state relation. Subscripts C, L, V1 and V2 are used to distinguish quantities specific to the carrier gas, the liquid and the two evaporated species, respectively; whereas the subscript G refers to the carrier plus vapor gas phase mixture. In what follows ρ_G is the gas-phase density, u_i is the gas phase velocity, P_G is the thermodynamic pressure, Y_C, Y_{V1} and Y_{V2} are the mass fractions of the carrier gas and the two droplet species evaporated vapor fractions, the gas phase viscosity is μ_G (assumed constant), R_{V1}, R_{V2}

and R_C are the gas constants for the vapor species and the carrier gas, respectively, and λ_G and Γ_G are the gas phase thermal conductivity and Fickian diffusion coefficient, respectively.

2.1. Lagrangian droplet equations

The formulation adopted for the present analysis is a multicomponent extension of that utilized by Miller and Bellan (1999, 2000), Miller (2001) and Khatumria and Miller (2003) for single component droplet laden mixing layers which was chosen based on comparisons with experimental data presented by Miller et al. (1998). The formulation is extended here to include the effects of multicomponent droplets both in the individual droplet equations and in the gas-phase source terms. The extension of the model for multicomponent droplets involves taking into consideration the presence of two or more liquid species when deriving the individual droplet equations (using Raoult's law) and the source terms for the gas phase equations. Although other more accurate options exist for modeling multicomponent droplet evaporation (including complete resolution of the droplet interior flow), the chosen formulation captures the basic effects of preferential droplet evaporation pertinent to the present investigation. Experimental validation of the multicomponent aspects of the model may be found in Chen et al. (1997). The droplet model is presented in a form suitable for arbitrary numbers of liquid species; however, the following results will be limited to binary component droplets for the sake of simplicity. Furthermore, non-equilibrium vaporization effects are excluded as only relatively low evaporation rates are considered (Miller et al., 1998); however, nothing in the present formulation precludes the future addition of non-equilibrium effects. In what follows, primarily only alterations to the above referenced formulations due to multicomponent vaporization are presented; the reader is referred to these works for additional details.

The Lagrangian modeled equations describing the transient position (X_i), velocity (v_i), temperature (T_d) and mass (m_d) of a single droplet are

$$\frac{dX_i}{dt} = v_i, \tag{1}$$

$$\frac{dv_i}{dt} = \frac{F_i}{m_d} \quad \text{with } F_i = m_d\left(\frac{f_1}{\tau_d}\right)(u_i - v_i), \tag{2}$$

$$\frac{dT_d}{dt} = \frac{Q + \sum[\dot{m}_{d,\alpha}L_{V,\alpha}]}{m_d C_L} \quad \text{with } Q = m_d\left(\frac{f_2}{\tau_d}\right)\left(\frac{NuC_{p,G}}{3Pr_G}\right)(T_G - T_d), \tag{3}$$

$$\frac{dm_d}{dt} = \dot{m}_d = -m_d\left(\frac{1}{\tau_d}\right)\left(\frac{Sh}{3Sc_G}\right)\ln[1 + B_M], \tag{4}$$

where the subscript 'd' denotes individual droplet conditions, the droplet time constant for Stokes flow is $\tau_d = \rho_L D^2/(18\mu_G)$, ρ_L is the density of the liquid mixture, D is the droplet diameter, C_L is the heat capacity of the liquid mixture, the latent heat of evaporation for species α is $L_{V,\alpha}$, and $\dot{m}_{d,\alpha}$

is the vaporization rate for liquid species α. Additionally, the gas mixture heat capacity is calculated using a mass averaging; $C_{p,G} = \sum[Y_\alpha\ C_\alpha]$ (evaluated at the droplet location), where $C_{p,C}$, $C_{p,V1}$ and $C_{p,V2}$ are the constant pressure heat capacities of the carrier gas and vapor species, respectively ($C_{v,C}$, $C_{v,V1}$ and $C_{v,V2}$ are the corresponding constant volume heat capacities). The gas phase Prandtl and Schmidt numbers are $Pr_G = \mu C_{p,G}/\lambda$ and $Sc_G = \mu/(\rho\Gamma)$, respectively. The drag force is determined by the local "slip velocity" vector $u_{sl,i} = u_i - v_i$ (subscript 'sl' denotes slip variables), whereas the convective thermal energy transfer (Q) is driven by the local slip temperature ($T_{sl} = T_G - T_d$), and the evaporation rate [Eq. (4)] is driven by the mass transfer number; $B_M = (Y_s - Y_V)/(1 - Y_s)$ (subscript 's' denotes droplet surface conditions). Note that the gas phase variables u_i, T_G and Y_V correspond to the undisturbed flow conditions surrounding the droplets which are interpolated from the Eulerian numerical grid to the droplet location during the simulations. The "1/3 rule" is employed to calculate the far field vapor mass fraction; $Y_V = Y_s + 1/3(Y_{V1} + Y_{V2} - Y_s)$.

In Eq. (2), Stokes drag is empirically corrected for finite droplet Reynolds numbers ($Re_{sl} = \rho_G U_{sl} D/\mu_g$ is based on the slip velocity and $Re_b = \rho_G U_b D/\mu_G$ is based on the blowing velocity) using a previously derived correlation (f) (Miller and Bellan, 1999). Modeled forms for the Nusselt (Nu) and Sherwood (Sh) numbers and the evaporative heat transfer correction (β) are the same as used in the above mentioned references. The vaporization model requires the vapor molar fraction of each pure species α ($\chi_s^{\star,\alpha}$; the superscript ★ indicates conditions for a single component droplet) at the droplet surface which is obtained by equating the vapor and liquid fugacities (or chemical potentials) at the surface. For "low" pressure this yields $\chi_s^\star P_G = P_{sat}$, where the saturation pressure (P_{sat}) is given by the Clausius–Clapeyron relation:

$$\chi_{s,\alpha}^\star = \frac{P_{atm}}{P_G} \exp\left[\frac{L_{V,\alpha}}{R_\alpha}\left(\frac{1}{T_{B,\alpha}} - \frac{1}{T_d}\right)\right], \tag{5}$$

where P_{atm} is atmospheric pressure, $T_{B,\alpha}$ is the normal boiling temperature of species α, [i.e. $T_{sat}(P_{atm})$]. At any given time, the gas-phase species mole fraction at the droplet surface can be obtained by means of Raoult's law:

$$\chi_{s,\alpha} = \chi_{l,\alpha}\chi_{s,\alpha}^\star, \tag{6}$$

where $\chi_{l,\alpha}$ is the liquid phase mole fraction of species α within the droplet. Finally the vapor surface mass fraction of species, α, is calculated directly from the molar fraction:

$$Y_{s,\alpha} = \frac{\chi_{s,\alpha} W_{V,\alpha}}{\sum[\chi_{s,\beta} W_{V,\beta}]}. \tag{7}$$

Finally, the fractional evaporation rate of species α is given by

$$\dot{m}_{d,\alpha} = \frac{Y_{s,\alpha}}{\sum\limits_L Y_{s,\beta}} \dot{m}_d, \tag{8}$$

where the denominator is the summation of the surface mass fractions for all liquid species present in the droplet. For very small droplets evaporating in high temperature conditions, non-equilibrium effects can be included in the model through a correction term added to the definition of the surface mole fractions (Miller et al., 1998).

2.2. Phase coupling

Phase coupling terms for the Eulerian gas phase transport equations for continuity, momentum, total energy, and the Species 1 and 2 vapor mass fractions are:

$$S_{\mathrm{I}} = -\sum_{\alpha}\left\{\frac{w_\alpha}{\Delta x^3}\left[\dot{m}_{\mathrm{d}}\right]_\alpha\right\}, \tag{9}$$

$$S_{\mathrm{II},i} = -\sum_{\alpha}\left\{\frac{w_\alpha}{\Delta x^3}\left[F_i + \dot{m}_{\mathrm{d}} v_i\right]_\alpha\right\}, \tag{10}$$

$$S_{\mathrm{III}} = -\sum_{\gamma}\left\{\frac{w_\gamma}{\Delta x^3}\left[v_i F_i + Q + \dot{m}_{\mathrm{d}}\left\{\frac{v_i v_i}{2}\right\} + \sum_{L}\left\{\dot{m}_{\mathrm{d},i} h_{\mathrm{V,s},i}\right\}\right]_\gamma\right\}, \tag{11}$$

$$S_{\mathrm{IV}} = -\sum_{\gamma}\left\{\frac{w_\gamma}{\Delta x^3}\left[\dot{m}_{\mathrm{d},1}\right]_\gamma\right\}, \tag{12}$$

$$S_{\mathrm{V}} = -\sum_{\gamma}\left\{\frac{w_\gamma}{\Delta x^3}\left[\dot{m}_{\mathrm{d},2}\right]_\gamma\right\}, \tag{13}$$

respectively. The summations are over local individual droplet contributions. The individual droplet evaporation rate ($\dot{m}_{\mathrm{d}}$), drag force (F_i) and heat flux (Q) are specified by the modeled droplet equations (Eqs. (2)–(4)), and $h_{V,s,\alpha}$ is the enthalpy of the evaporated vapor at the droplet surface for species α. Extending the single component formulation of Miller and Bellan (1999), the surface enthalpy is $h_{\mathrm{V,s},\alpha} = C_{\mathrm{p},\alpha} T_{\mathrm{d}} + h^0_{\mathrm{V},\alpha}$ for calorically perfect species, where $h^0_{\mathrm{V},\alpha}$ is a constant reference enthalpy calculated from the latent heat evaluated at the boiling temperature for each species; $h^0_{\mathrm{V},\alpha} = L_{\mathrm{V},\alpha}(T_{\mathrm{B},\alpha}) + (C_{\mathrm{L},\alpha} - C_{\mathrm{p},\alpha}) T_{\mathrm{B},\alpha}$. Once the reference enthalpies are determined, the latent heat takes the consistent linear form; $L_{\mathrm{V},\alpha} = h^0_{\mathrm{V},\alpha} - (C_{\mathrm{L},\alpha} - C_{\mathrm{p},\alpha})$ (see Miller and Bellan, 1999 for additional details).

The local summations appearing in the above coupling source terms are necessarily grid dependent functions; the summations are over all droplets (subscript γ indicates the individual droplet variables; no summation over Greek indices) residing within a local numerical discretization area (Δx^2). A geometric weighting factor, w_γ, is used to distribute the individual droplet contributions to the four nearest neighbor surrounding grid points (i.e. corners of the computational area Δx^2). The point particle assumption and resulting interpolations onto the Eulerian grid are well known to introduce some level of "modeling" approximations into the formulation. Limitations of the approach have been well documented in Miller and Bellan (1999, 2000), Miller (2001), Khatumria and Miller (2003) and are the same for the present binary component droplets. The reader is referred to the above for discussions.

3. Procedure and approach

The flow configuration considered is that of a 2D mixing layer formed by the merging of a pure-gas stream with a binary component droplet laden, parallel-flowing stream. The planar mixing layer configuration presents a relatively simple non-homogeneous flow geometry for turbulent mixing layer studies. A 2D flow is considered due to the prohibitive computational expense of capturing true transition to turbulence in a three-dimensional two-phase mixing layer (Miller and Bellan, 2000; Miller, 2001). Although not truly turbulent, the present 2D simulations allow the incorporation of up to eight initial vortical structures with four associated pairings, and therefore yield a highly convoluted mixing region sufficient for the present purposes of investigation. The approach used for the 2D mixing layer simulations is the same as in Miller (2001) and Khatumria and Miller (2003). The present section defines the mixing layer geometry, the numerical approach, and all properties.

3.1. Mixing layer configuration and approach

Fig. 1 shows a schematic of a temporally developing mixing layer (boxed region). The streamwise (x_1) and cross-stream (x_2) domain lengths are L_1 and L_2, respectively. The boundary conditions are periodic in the streamwise direction, whereas adiabatic slip-wall conditions are used for the cross-stream (x_2) boundaries. The "upper stream" ($x_2 > 0$) is a pure gas phase flow with parameters denoted by the subscript 'US', whereas the initially laden "lower stream" ($x_2 < 0$; subscript 'LS') is randomly seeded with binary component droplets, with uniform mean number density profile as a function of x_2. The lower stream either has pure carrier gas laden with droplets or a mixture of fuel vapor and carrier gas laden with droplets. The initial vorticity thickness is $\delta_\omega(t) = \Delta U_0/\langle\partial u_1/\partial x_2\rangle_{max}$; the brackets $\langle\rangle$ indicate averaging over the homogeneous x_1 direction, and the mean velocity difference across the layer, $\Delta U_0 = U_1 - U_2$, is calculated from a specified value of the convective Mach number (M_c) (Papamoschou and Roshko, 1988).

The base flow mean velocity, temperature and number density are specified based on an error function profile; $\mathrm{erf}(\pi^{1/2}x_2/\delta_{\omega,0})$ (Moser and Rogers, 1991) corresponding to the similarity solution for constant density incompressible flow. Sinusoidal velocity perturbations are superimposed on the base flow profile having wavelengths of the same form and amplitudes as used by Khatumria and Miller (2003). The non-dimensional forcing amplitude ($F^{\star}_{2D}$) is characterized by the spanwise circulation of the disturbance relative to the base flow circulation ($\lambda_1\Delta U_0$). The imposed distur-

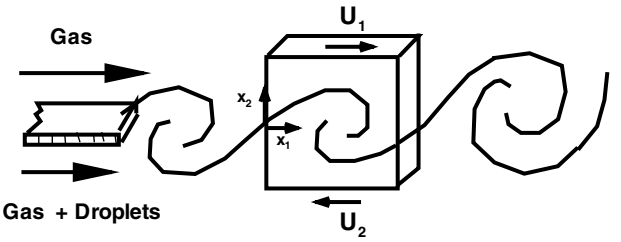

Fig. 1. Schematic of the two-phase temporally developing mixing layer (boxed region, above).

bances instigate the development of eight initial vortices together with four pairing events prior to the physical intervention of the domain boundaries. Note that all base gas phase flow conditions are identical for all simulations discussed below and correspond to uniform density low Mach number flows. Therefore, effects due to not using base flow profiles determined from similarity analysis or actual most unstable forcing wavelengths will be minimal and the same for all base gas phase flows. Similarity and linear stability analysis have not been performed for two-phase mixing layers of the type considered here to the authors knowledge. In light of this, and due to the fact that no results are presented pertaining to mixing layer growth rates or other associated quantities directly affected by the flow forcing wavelength, the present approach is deemed acceptable.

3.2. Numerical procedure

The present study employs an explicit fourth-order accurate Runge–Kutta temporal integration (Kennedy and Carpenter, 1994) (for both the gas phase and the Lagrangian droplet equations) coupled with an eighth-order accurate central finite difference scheme in the streamwise direction (x_1), a fourth order accurate tridiagonal compact finite difference in the cross-stream direction (x_2), and a tenth order accurate filter function to control grid scale numerical errors. The Lagrangian droplet transport equations, Eqs. (1)–(4), require the knowledge of the gas phase flow variables evaluated at the local droplet positions. In general these locations do not coincide with the grid point locations; therefore, a fourth order Lagrange interpolation procedure is used. Specification of the time step for each temporal iteration is based on consideration of both a maximum Courant number and on the droplet time constant such that initially $\Delta t/\tau_{d,0} < 0.1$. When the droplet's Stokes number reaches $St = \tau_d \Delta U_0/\omega_{\omega,0} = 0.05$, evaporation is stopped and the droplet is removed from the calculation, so as not to render Δt too large relative to the droplet time scale. All the simulations are conducted with a simulation time step calculated based on a maximum Courant number of $C = 0.5$.

The source terms in the gas-phase conservation equations, Eqs. (9)–(13), are necessarily grid-dependent functions. In order to evaluate the contributions of all surrounding droplets within the discretization range, the summation is over geometrically weighted (w_γ) contributions from all individual droplets (denoted by γ). The resulting source terms are then minimally smoothed using a local procedure whereby the source at each individual grid node is shifted toward the surrounding six nearest node average (with coefficient 0.75) (Miller and Bellan, 1999). This procedure is found to be necessary owing to the spatial "spottiness" of the source terms which can lead to artificial oscillations with non-dissipative central differencing schemes.

3.3. Flow parameters and properties

The dimensions of the numerical domain considered are $L_1 = L_2/1.125 = 0.2m$. The elongated cross-stream domain size reduces boundary condition effects and provides adequate room for the mixing layer to grow. The convective Mach number is chosen to be $M_c = U_0/\sqrt{R_c T_0 C_{p,C}/C_{v,C}} = 0.35$ (T_0 is the initial uniform temperature in a stream). This choice is justified based on the linear stability analysis performed by Sandham and Reynolds (1989) which showed that compressible instability modes are not significant for $M_c < 0.6$, and also by the DNS

performed by Samimy and Lele (1991) of the dispersion of solid particles in a 2D planar mixing layer which found no significant compressibility effects on the dispersion process for $0.2 \leqslant M_c \leqslant 0.6$. The initial Reynolds number is $Re_0 = \rho_{G,0}\Delta U_0 \delta_{\omega,0}/\mu_G = 450$, and the initial flow is isobaric with $P_0 = P_{atm}$ and isothermal with $T_{G,0} = 375$ K. The initial droplet slip velocity is zero, the initial diameter (D_0) is based on a specified value for St_0, and the constant initial droplet temperature is $T_{d,0} = 350$ K unless otherwise specified. The initial mass fraction for both species in the binary component droplets is 0.5. The above set of parameters are chosen in order to yield evaporation time scales approximately equal to the mixing-layer growth time scale; the limiting behavior of very slow (or rapid) evaporation rate is similar to solid particle (or single phase) flow, and is therefore of limited interest. The grid resolution is 512×576 grid points for all cases. The normalized forcing amplitude is $F_{2D} = 0.1$.

As mentioned above, the "lower stream" is randomly seeded with binary component droplets with initial diameter calculated based on a specified Stokes number. The mass loading ratio for the lower stream is defined as the total liquid to gaseous mass:

$$ML_0 = \frac{N_p m_p}{\rho_G L_1 L_2 L_3'/2}, \tag{14}$$

where N_p is the number of droplets. In the above, a reference length in the x_3 direction is required to define a meaningful mass loading ratio for a 2D flow. A model developed by Miller (2001) assuming a Cartesian distribution of droplets is used here. According to the model, the spanwise length scale L_3' is defined by equating the assumed Cartesian particle grid area to the total area of the laden stream:

$$N_p L_3'^2 = \frac{L_1 L_2}{2}. \tag{15}$$

All species properties are listed in Table 1. The carrier gas species is chosen to have properties corresponding to those of air for all the simulations. All the properties for the droplet liquid and vapor species are treated as constant and are evaluated at the boiling temperature (Miller et al., 1998). The Lewis number (Le_G) is assumed to be unity (i.e. $Sc_G = Pr_G$). However, in order to provide a high fidelity resolution of the flow, the gas phase viscosity is defined using an artificially inflated value calculated from a specified Reynolds number, Re_0. In this sense, the species are essentially "pseudo-species;" however, effects of realistic air-droplet species molecular weight ratios, heat capacity ratios, boiling temperatures and latent heat values are retained.

Table 1
Species latent heats, boiling temperatures, liquid densities and molecular weights

Species	L_V [J kg^{-1}]	T_{BOIL} [K]	ρ_L [kg/m^3]	W_V [kg (kg mole)$^{-1}$]
Heptane	3.16×10^5	371.6	649.38	100.0
Decane	2.79×10^5	447.7	642.0	142.0
Hexane	3.34×10^5	344.6	664.0	86.178
TCA	2.85×10^5	347.2	1339.0	133.405
Water	2.26×10^6	373.15	997.0	18.015

4. Results

The computational model developed is used to: (1) study the vaporization characteristics of a single isolated binary-component droplet, (2) discuss the potential role of the species latent heats of vaporization in determining relative volatilities (in addition to the traditionally cited boiling temperature; Sangiovanni and Kesten, 1976; Law, 1990; Kim et al., 1990; Kramlich, 1990; Presser et al., 1992), and (3) study the development of a planar mixing layer with one stream laden with binary component droplets. Results are first presented for single droplets evaporating in infinite quiescent environments. These simulations are conducted under identical thermodynamic and property conditions used in the following mixing layer simulations. These single droplet simulations are useful for directly illustrating the base underlying physics of both preferential vaporization and latent heat influence on determining relative volatilities isolated from the more complex flow couplings within the mixing layer. The mixing layer simulations are then used to address the influence of transient and vortical flow couplings to the vaporization processes including the effects of flow saturation due to build up of gas phase vapor fractions and latent heat induced temperature reductions.

4.1. Single droplet vaporization

Numerical solutions of the governing equations for a single stationary isolated droplet vaporizing in a quiescent air environment are first solved for single and binary component droplets [Eqs. (3) and (4)]. Three different pairs of species are chosen based on studies discussed below in order to explore the effects of various controlling parameters involved in the vaporization of a multicomponent droplet. The reasons for choosing to investigate the particular species, and species pairs, listed in Tables 1 and 2 are first considered. All properties and scales used to nondimensionalize variables correspond to those used for the mixing layer simulations described below. Therefore, the results presented in this section should only be interpreted as being relevant to the (low Reynolds number) mixing layer simulations, and not quantitatively correct for droplets evaporating in real air.

From the droplet temperature [Eq. (3)] and droplet mass [Eq. (4)] equations, it is evident that the slip temperature ($T_G - T_d$) and the slip mass fraction ($Y_s - Y_V$) are the two dominant parameters controlling the droplet evaporation. The surface mass fraction of a particular species in relation to the mass fraction of that species far away from the surface determines the mass transfer potential, B_M, which in turn controls the droplet evaporation rate. Fig. 2 shows the surface mass fractions of different (pure) species plotted against droplet temperature for the vaporization of a pure liquid species droplet in quiescent air at 375 K. The data are obtained through the solution of

Table 2
Ratios of the latent heats and boiling temperatures for the three pairs of species under consideration

Species A–B	$\frac{L_{V,A}}{L_{V,B}}$	$\frac{T_{B,A}}{T_{B,B}}$
Heptane–decane	1.13	0.83
Hexane–TCA	1.17	0.993
Water–heptane	7.14	1.004

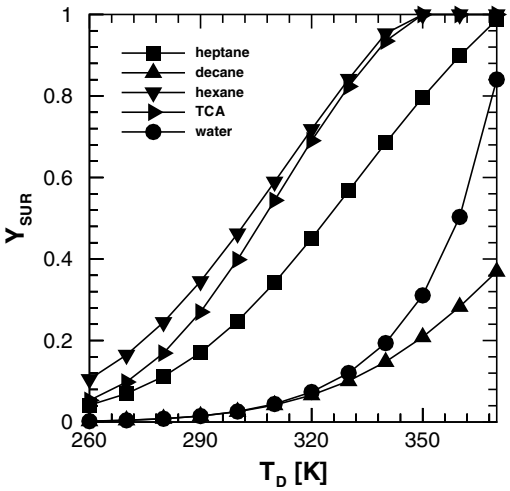

Fig. 2. Surface mass fractions on a single isolated single component droplet for different species as a function of droplet temperature.

Eqs. (5)–(7) and represent the relative volatilities of the individual species as a function of droplet temperature. Based on the results of Fig. 2 and on Tables 1 and 2, three pairs of species are identified for the present study in order to investigate the vaporization of a typical binary-component droplet and also to study the effects of the latent heats of vaporization of the two species on the vaporization characteristics of the droplet. For the sake of simplicity, only pure species droplets and 50/50 by mass binary component droplets are considered. Three binary species pairs are chosen as indicated in Table 2; heptane–decane, hexane–TCA, and water–heptane. Both hexane and TCA have relatively large volatilities relative to the other species at fixed temperature due to their lower boiling temperatures. Preferential diffusion effects would also be expected to be minimal for mixtures of these species due to their nearly equal surface mass fractions. The heptane–decane species pair is chosen for having substantial preferential diffusion affects related to varying boiling temperatures. In contrast, water and heptane have approximately the same boiling temperatures; however, their surface mass fractions are quite different owing to a very large variation in their latent heats (Table 1). As will be shown, this latent heat difference results in substantial preferential vaporization despite nearly equal boiling temperatures.

Fig. 3 shows the temporal evolution of the normalized surface area and the temperature for a single isolated 50% by mass heptane–decane droplet compared to pure heptane and pure decane droplet cases (having the same initial Stokes number, $St_0 = \tau_{d,0}\Delta U_0/\delta_{\omega,0} = 2.0$). The droplets have an initial temperature $T_{d,0} = 350$, and are evaporating in a quiescent air environment at $T_G = 375$ K. Time is normalized by the flow time scale of the corresponding mixing layer simulation defined as $t^\star = t\Delta U_0/\delta_{\omega,0}$ (the "eddy turnover time;" see below). Initially a rapid decay in the droplet temperature is observed as the droplet attempts to equilibrate towards the "wet bulb" temperature. For single component droplets the wet bulb temperature is a quasi-steady depressed droplet temperature approached after initial transients due to a balance between droplet heating and latent heat effects. However, for multicomponent droplets the process is more com-

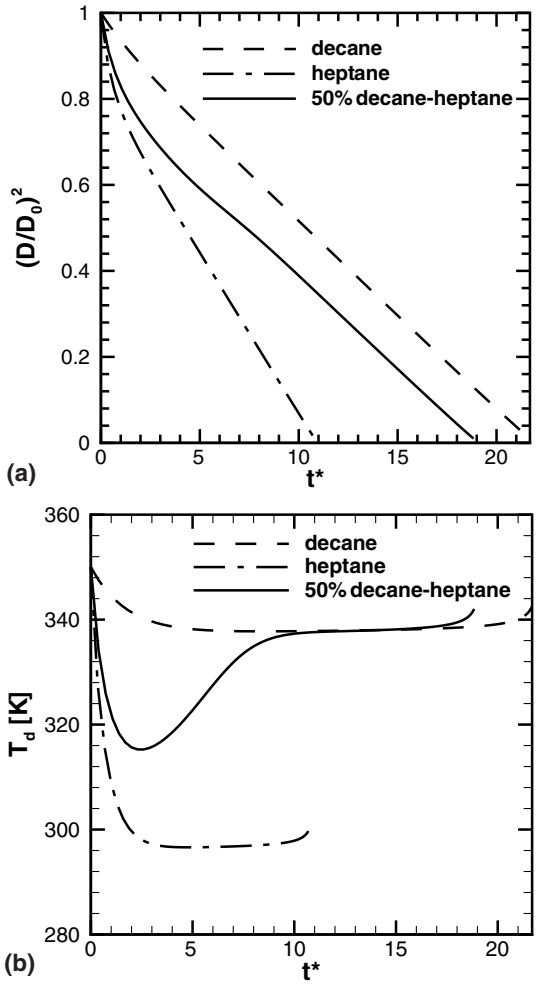

Fig. 3. Temporal evolution of the: (a) normalized droplet projected surface area, and (b) the droplet temperature for both pure and multicomponent heptane and decane droplets.

plex since the surface mass fractions and temperatures are dependent on the liquid mass fraction and also on the difference in the volatilities of the liquid species. During the early stages of evaporation, heptane, being the more volatile species, as indicated by its lower boiling temperature, dominates the vaporization of the binary component heptane–decane droplet (Fig. 3). After this initial period, the droplet settles down to a quasi-steady temperature of approximately 340 K. It is observed that the heptane component is preferentially vaporized until $t^{\star} \approx 10$, after which only the decane remains and continues vaporizing as a pure component droplet. This behavior is consistent with previous experimental results (e.g. Wood et al., 1960).

The droplet Stokes number is also an important parameter governing evaporation. However, the isolated droplet equations are linear in St and the Stokes number affects the total evaporation time period but does not significantly alter the basic behavior of droplet evaporation. The value

$St_0 = 2.0$ is chosen for the study of the temporal mixing layer since both dispersion and the preferential concentration phenomenon (whereby the droplets are preferentially concentrated in high strain regions of the flow) are maximized. Note, however, that the total evaporation time may be substantially extended in the mixing layer simulations due to both build up of vapor concentration in the free stream (Y_V) and cooling of the gas due to latent heat effects, which are not accounted for in the present single droplet simulations.

Figs. 4 and 5 show the temporal variation of the normalized droplet surface area and temperature for 50% hexane–TCA and 50% heptane–water droplets evaporating in quiescent air at $T_G = 375$ K. The results are compared to the vaporization of pure species droplets in each case. The initial droplet Stokes number is fixed at $St_0 = 2.0$ for both cases, and the initial droplet temperatures are 340 K and 350 K, respectively (340 K is chosen for hexane–TCA case in

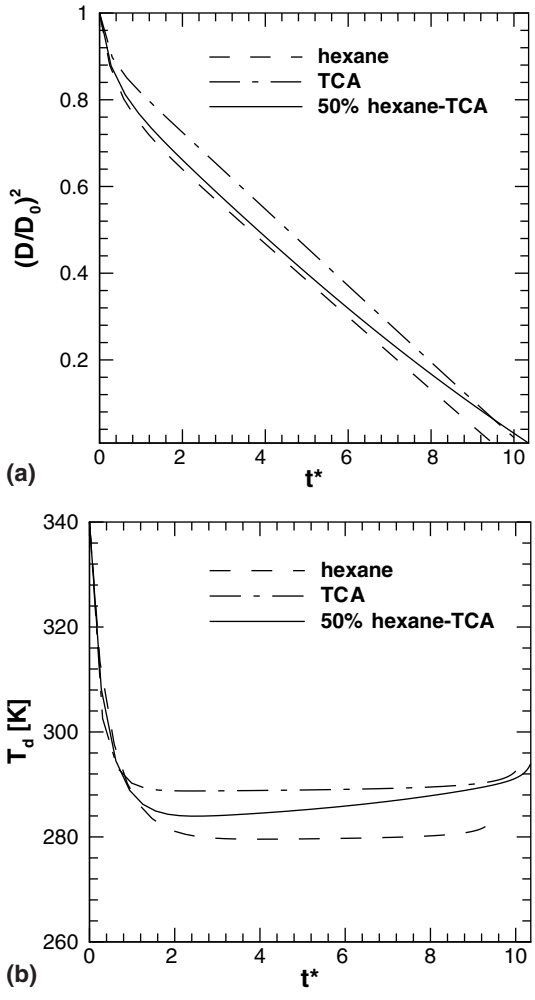

Fig. 4. Temporal evolutions of the normalized droplet: (a) surface area and (b) droplet temperature for 50% hexane–TCA droplet compared to pure hexane and pure TCA droplets.

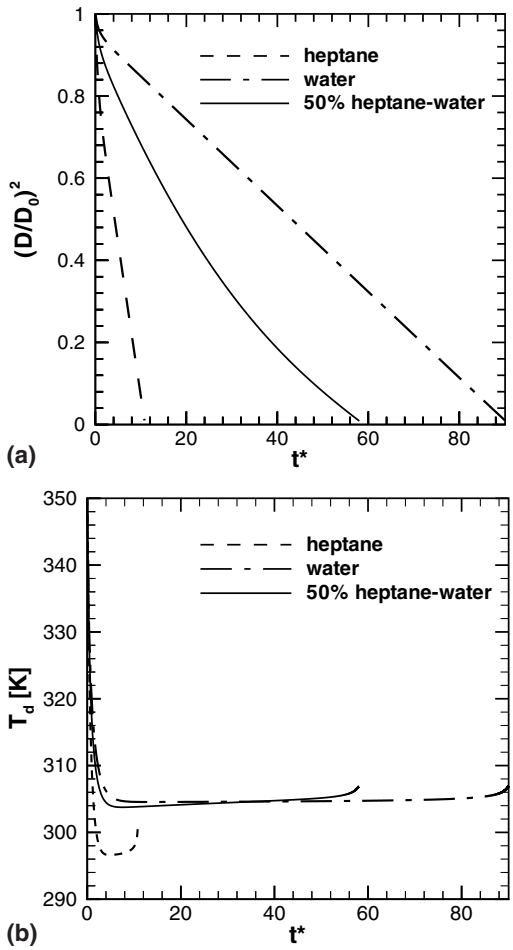

Fig. 5. Temporal evolutions of the normalized droplet: (a) surface area and (b) droplet temperature for 50% heptane–water droplet compared to pure heptane and pure water droplets.

order to not exceed the boiling temperatures of the pure liquid species). The results from these plots reveal that the latent heat of vaporization plays a dominant role in the vaporization behavior of the droplets. In the first case, all three curves show similar behavior. It is observed that hexane is slightly more volatile owing to its lower boiling point even though it has a slightly higher latent heat of vaporization. The 50% hexane–TCA curve shows preferential vaporization of hexane to a small extent. Fig. 5 shows that the heptane and water show very different vaporization behaviors even though both have almost equal boiling temperatures. This is because of the significant difference in their latent heats of vaporization. Therefore, it can be inferred that the latent heat of vaporization also plays an important role in determining species volatility apart from the boiling point, which is usually considered to be the primary measure of volatility. Both the latent heat and the boiling temperature must be considered when estimating relative volatilities.

Table 3
Simulation parameters including the initial droplet mass loading ratio, volumetric loading ratio, Stokes number, number of drops and number of drops per grid point in the laden stream, and the ratio of the initial droplet size to the grid spacing

Run	ML_0	VL_0	St_0	N_p	$N_p^\star$	$D_0/\Delta x$	Comments
0	0	–	–	–	–	–	Single phase
1	0.25	3.87×10^{-4}	2.00	128,700	0.873	0.0948	Decane–heptane
2	0.25	2.50×10^{-4}	2.00	139,500	0.946	0.0840	Heptane–water
3	0.25	3.04×10^{-4}	2.00	149,000	1.01	0.0761	Hexane–TCA

All Runs have 512×576 grid points with $M_c = 0.35$, $Re_0 = 450$, $T_{G,0} = 375$ K and $T_{d,0} = 340$ K.

4.2. Droplet laden mixing layer

The single droplet simulation results presented above provide insight into how binary component droplets will behave when added to a two-phase mixing layer. Table 3 presents the parameters of the mixing layer simulations which were performed for this study. The primary parameters describing the simulations are the liquid mass loading ratio, the volumetric droplet loading ratio (VL_0; ratio of the liquid volume to the gas volume in the laden stream), initial droplet Stokes number, and the liquid species composition. Several flow variables are fixed for all simulations; the initial gas temperature is uniform with $T_{G,0} = 375$ K, the flow Reynolds number is $Re_0 = 450$, the flow Mach number is $M_C = 0.35$, and for two-phase cases the initial droplet temperature is $T_{d,0} = 350$ K. All simulations utilize 512×576 finite difference grid points in the x_1 and x_2 directions, respectively. Droplets are initially monodisperse binary component liquids with 50% by mass allocations of each species listed in Table 3. For the sake of simplicity, we present only results corresponding to fixed initial liquid mass loading ratio $ML_0 = 0.25$ and initial droplet Stokes number $St_0 = 2.0$. Variations of these parameters were observed to produce the same effects on the mixing layer development as previously reported by Miller and Bellan (1999) for a single component droplet laden mixing layer. That is, the mixing layer growth rate is increasingly retarded for increasing mass loadings, whereas only negligible changes in the growth rate are observed while varying the Stokes number in the range $0.25 \leqslant St_0 \leqslant 12$. We therefore fix these parameters for the present investigation; however, additional results pertaining to changes in ML_0 and St_0 may be found in Varanasi (2001).

Fig. 6(a) depicts contours of the instantaneous droplet number density in the mixing layer domain at the final simulation time illustrating the droplet distribution within the developed two-phase flow laden with 50/50 heptane–decane droplets (Run 1). The number density is calculated as an Eulerian field using the instantaneous Lagrangian droplet locations:

$$n = \sum_{\alpha} \frac{w_\alpha}{\Delta x^3}, \tag{16}$$

where w_α is the weighting parameter described described previously. Preferential concentration of the droplets is evident in Fig. 6(a); the spanwise vortical regions formed by the vortex pairing are essentially devoid of droplets. Concentration "streaks" of increased droplet number density are observed around the periphery of the vortex regions. These configurations are explained by the droplets being centrifuged away from the high vorticity regions in the fluid

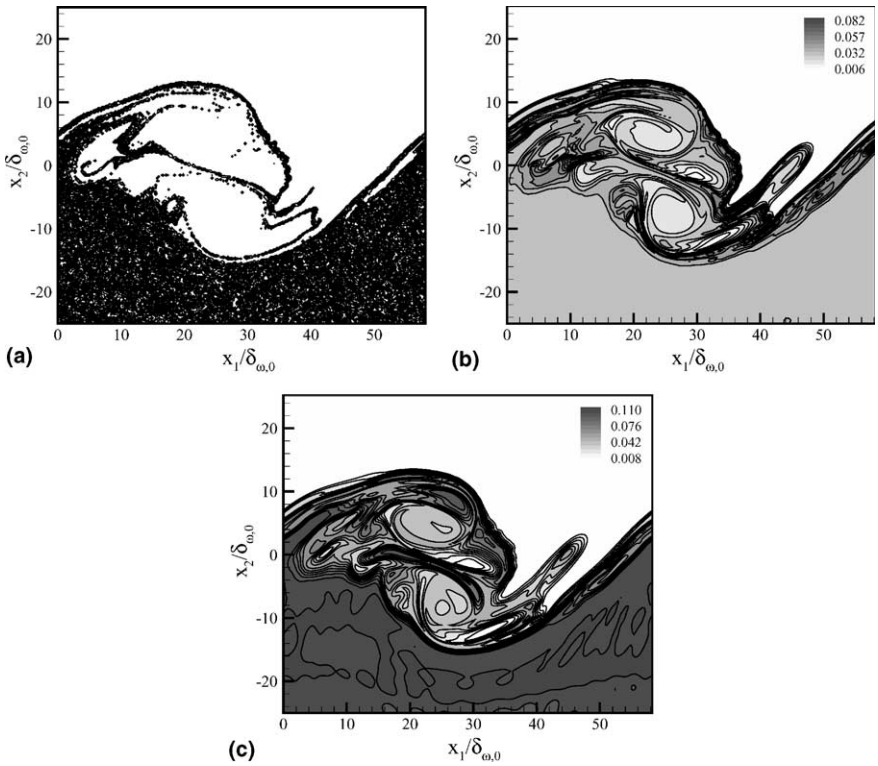

Fig. 6. Instantaneous contour plots of the: (a) Eulerian number density; (b) decane vapor mass fraction and (c) heptane vapor mass fraction from Run 1 at simulation time $t^\star = 180$.

owing to inertia, and converging into the high strain "convergence" regions of the flow. Similar concentration streaks have been previously observed both for solid particles (Martin and Meiburg, 1994; Kiger and Lasheras, 1997) and for single component evaporating droplets (Miller and Bellan, 1999). In the case of vaporizing droplets, these previous studies have observed that the laden stream temperature is reduced due to latent heat effects, resulting in a temperature stratified mixing layer from initial isothermal conditions (see below). The streak structures therefore act to bring the evaporating droplets into close contact with the relatively higher temperature fluid between the primary vortical rollers, thereby enhancing local evaporation rates.

Fig. 6(b) and (c) shows the instantaneous mass fraction contours of decane and heptane for Run 1, respectively, at the same time as the number density shown in Fig. 6(a). The figures show high vapor mass fractions around the outer periphery of the vortical structures, with a maximum in the strained regions. As previously mentioned, this is caused by higher evaporation rates due to contact with the relatively higher temperature upper stream fluid in the streak regions. A comparison between the decane and heptane mass fractions shows the effect of preferential vaporization on the vapor mass fractions. Heptane, being the more volatile species, evaporates most rapidly during the initial stages resulting in significantly higher vapor mass fractions compared to decane; see also Fig. 3.

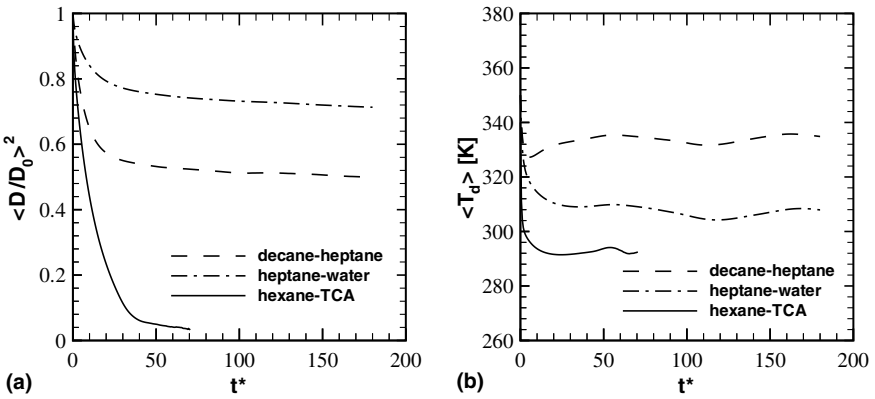

Fig. 7. Temporal evolution of the: (a) normalized mean droplet diameter squared and (b) mean droplet temperature ($ML_0 = 0.25$, $St_0 = 2.0$; Runs 1, 2 and 3).

In Fig. 6(b) and (c) both components have reached a state of saturation in the free stream resulting from both decreasing gas phase temperatures (due to latent heat effects) as well as elevated free stream vapor mass fractions accumulated by the evaporating droplets. Both effects were absent in the previous isolated droplet simulations. This evaporative flow saturation is illustrated more clearly in Fig. 7 which depicts the mean droplet areas and temperatures as a function of time for all three mixing layer simulations. The averages are over the entire domain and are therefore dominated by contributions from droplets residing in the free stream. Evaporative saturation is observed for both the decane–heptane and the heptane–water droplet laden flows as indicated by a near cessation of further decreases in droplet sizes after time $t^\star \approx 30$. In contrast, both TCA and hexane are much more volatile and are able to continue through to complete vaporization even in the free stream by $t^\star \approx 70$. Both hexane and TCA have relatively low boiling temperatures and therefore exhibit reduced long time droplet temperatures compared to the remaining species with larger boiling temperatures. After completion of evaporation the hexane–TCA droplet laden flow evolves as a single-phase mixing layer flow.

Fig. 8 shows the cross-stream averaged vapor mass fractions of all droplet species for each of the simulations at the final time of $t^\star = 180$. The steep gradients for the mass fractions for $x_2/\delta_{\omega,0} > -10$ are due to increased rates of evaporation caused by the droplets in the strained fluid region coming into contact with the higher temperature fluid in the unladen stream. A relatively steeper gradient is observed for the more volatile species when preferential diffusion is present (Fig. 8(a) and (b)). For example, for decane–heptane droplets in Run 1, preferential evaporation of heptane during the initial stages of the mixing layer development yields enhanced levels of free stream vapor heptane. During the later stages when only decane remains and continues to evaporate, the mixing layer thickness grows and more droplets are entrained into the layer; thereby increasing the mass fraction of decane. Fig. 8(b) and (c) illustrates the cross-stream averaged mass fractions from instantaneous mixing layer results for Run 2 and Run 3 at the final simulation time, $t^\star = 180$, respectively. It is observed that the vapor mass fractions of heptane and water are very different from one another while those of hexane and TCA are almost the same. This result is consistent with the results for single droplet vaporization for these pairs where it was con-

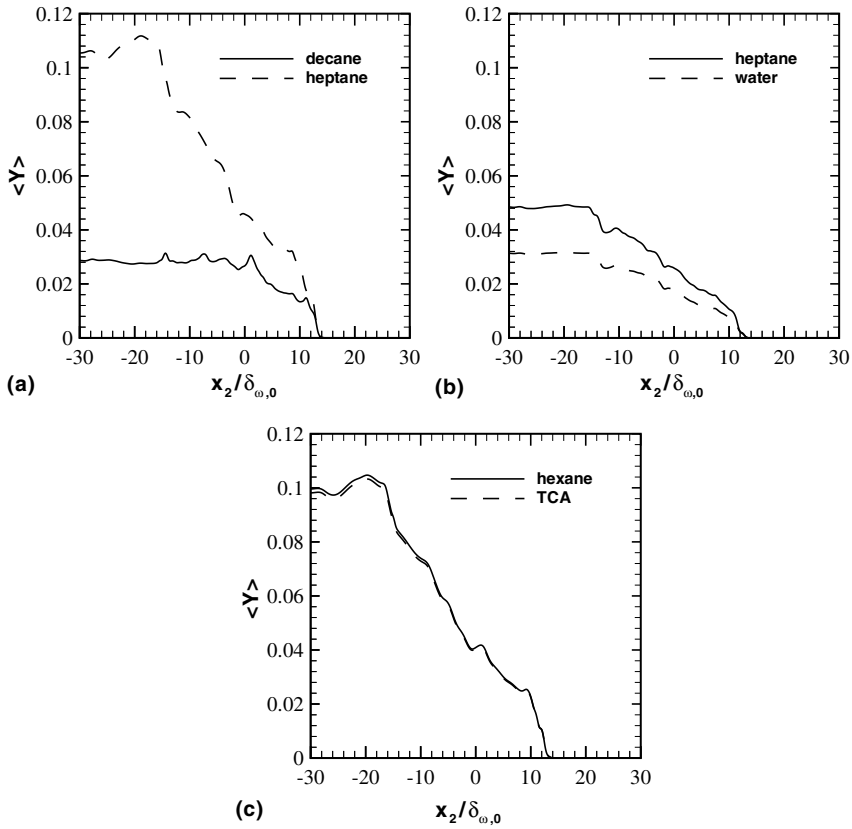

Fig. 8. Mean cross-stream evaporated vapor mass fractions at time $t^{\star} = 180$ for simulations: (a) Run 1; (b) Run 2 and (c) Run 3 with $ML_0 = 0.25$ and $St_0 = 2.0$.

cluded that the latent heat of vaporization plays an important role in determining the species volatility (see Figs. 4 and 5). Note, the heptane and water vapor fractions in the free stream differ significantly less than might be expected from the corresponding single droplet simulations. This occurs due to the relatively large latent heat of water substantially reducing the gas phase temperature, and thereby the vaporization rates (see below).

Finally, Fig. 9 illustrates the influence of gas phase cooling on the saturation process through examination of the cross-stream averaged gas phase temperatures corresponding to the results of Fig. 8. Results for the single phase mixing layer (Run 0) are also shown. A comparison of the single phase and two-phase mean flow temperatures illustrates the evaporative cooling effects of the droplets owing to their latent heats. Water has the largest latent heat of the species considered in this study and droplets containing water may be expected to yield the largest reduction in free stream gas temperatures. However, Fig. 9 shows that the hexane–TCA droplets produce a nearly equal reduction in the gas temperature. This is attributed to the fact that the heptane–water droplets reach early flow saturation. In contrast, the hexane–TCA droplets were able to completely vaporize, thus contributing their entire potential latent heat thermal energy absorption to the

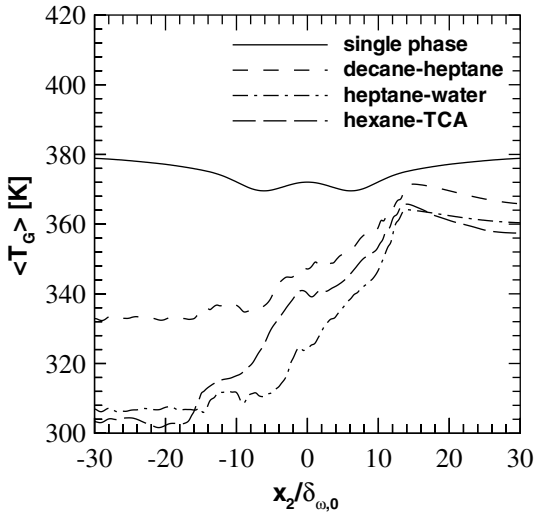

Fig. 9. Mean cross stream gas phase temperature for Runs 0, 1, 2 and 3 at time $t^{\star} = 180$.

flow. This is another indication of the complex nature of multicomponent droplet evaporation in turbulent flows.

5. Conclusions

Results have been presented from simulations of a 2D, temporally developing mixing layer with one stream laden with binary component droplets. The simulations were conducted in the Eulerian–Lagrangian reference frame in which every individual droplet is tracked through the solution of time-dependent equations for each droplet position, velocity, temperature and mass. An appropriate evaporation model was developed based on an infinite diffusion classical rapid mixing model and Raoult's law. Complete two-way coupling was incorporated between the two phases. The derived governing equations were solved for: (1) a single evaporating binary component droplet, and (2) a 2D temporally developing mixing layer with one binary component droplet laden stream. Simulations were conducted under fixed flow conditions to examine the effects of preferential multicomponent vaporization.

Three different pairs of species were identified to examine several controlling parameters involved in multicomponent droplet vaporization. The species chosen for their representative properties were heptane, hexane, decane, TCA and water. Preferential vaporization of the more volatile species was illustrated for single isolated binary component droplets, evaporating in a quiescent environment. The initial droplet diameter had little effect on the vaporization behavior of the droplet, though it changes the evaporation time scale in a manner consistent with the "D^2 law". An examination of the parameters governing the relative volatilities of the evaporating species revealed that the latent heat is an important parameter to be considered in determining the "true" volatility of a species. For example, heptane and water mixtures, having essentially equal boiling temperatures, exhibit relatively strong preferential vaporization of the heptane due to the

much larger latent heat associated with water. Both the boiling temperatures and the latent heats of species therefore need be considered in estimating volatilities.

Simulations were then conducted to study the effects of preferential vaporization, evaporative flow saturation, preferential concentration, and flow modulation in a 2D temporally developing mixing layer. Both flow visualizations and quantitative graphical results were used to study the instantaneous flow structure during different stages of evolution of the mixing layer. Preferential concentration of droplets in the high strain convergence regions in the flow was observed. Concentration streaks were observed to form in the strained fluid regions between the spanwise vortices similar to previous results for solid particle and single-component droplet-laden mixing layer investigations. Relatively large evaporation rates are observed in these streak structures due to the contact of droplets with relatively higher temperature fluid in the unladen stream. This leads to elevated vapor mass fractions in these regions. Marked differences were observed in the evaporated vapor mass fraction concentrations within the mixing layer due to preferential vaporization. Cross-stream profiles of the mean vapor mass fractions show steeper gradients within the mixing layer because of the preferential concentration of droplets around the periphery of the large scale vortical structures. Evaporative flow saturation is observed in the laden stream due to the build up of vapor mass fraction and the decrease in the gas temperatures due to latent heat effects. This process was found to be more complex than in single component droplet studies owing to the relative species volatilities.

Acknowledgments

The research conducted at Clemson University was supported by the National Science Foundation through the Faculty Early Career Development Program; Grant CTS-9983762. Computational support was provided by the California Institute of Technology's Center for Advanced Computing Research (CACR) utilizing the Hewlett-Packard V2500, and by the Department of Mechanical Engineering at Clemson University on a Beowulf PC cluster.

References

Aggarwal, S.K., Peng, F., 1995. A review of droplet dynamics and vaporization modeling for engineering calculations. J. Eng. Gas Turbines Power 117, 453–461.

Aggarawal, S.K., Tong, A.Y., Sirignano, W.A., 1984. A comparison of vaporization models in spray calculations. AIAA J. 22, 1448–1457.

Bellan, J., Summerfield, M., 1978. Theoretical examination of assumptions commonly used for the gas phase surrounding a burning droplet. Combust. Flame 33, 107–122.

Chen, G., Aggarwal, S.K., Jackson, T.A., Switzer, G.L., 1997. Experimental study of pure and multicomponent fuel droplet evaporation in a heated air flow. Atom. Sprays 7, 317–337.

Chen, X.Q., Pereira, J.C.F., 1996. Computation of turbulent evaporating sprays with well-specified measurements: A sensitivity study on droplet properties. Int. J. Heat Mass Transfer 39, 441–454.

Crowe, C.T., Troutt, T.R., Chung, J.N., 1996. Numerical models for two-phase turbulent flows. Ann. Rev. Fluid Mech. 28, 11–43.

Godsave, G.A.E. 1953. Studies of the combustion of drops in a fuel spray: the burning of single drops of fuel. In: Proceedings of the 4th Symposium (International) on Combustion, pp. 818–830.

Kennedy, C.A., Carpenter, M.H., 1994. Several new numerical methods for compressible shear-layer simulations. Appl Numer. Math. 14, 397–433.
Khatumria, V.C., Miller, R.S., 2003. Numerical simulation of a fuel droplet laden exothermic reacting mixing layer. Int. J. Multiphase Flow 29, 771–794.
Kiger, K.T., Lasheras, J.C., 1997. Dissipation due to particle/turbulence interaction in a two-phase, turbulent, shear layer. Phys. Fluids 9, 3005–3023.
Kim, J.S., Lee, A., Law, C.K., 1990. On the gasification of droplets of azeotropic mixtures: theory and experiment. Proc. Combust. Inst. 23, 1423–1429.
Kramlich, J.C., 1990. Observations on waste destruction in liquid injection incinerators. Combust. Sci. Tech. 74, 17–30.
Landis, R.B., Mills, A.F., 1974. Effect of internal diffusional resistance on the evaporation of binary droplets. Proc. 5th Int. Heat Transfer Conf. 4, 345–349.
Lara-Urbaneja, P., Sirignano, W.A., 1981. Theory of transient multicomponent droplet vaporization in a convective field. In: Proceedings of the 18th Symposium (International) on Combustion, pp. 1365–1374.
Law, C.K., 1990. Considerations of droplet processes in liquid hazardous waste incineration. Combust. Sci. Tech. 74, 1–15.
Law, C.K., Prakash, S., Sirignano, W.A., 1977. Theory of convective, transient, multicomponent droplet vaporization. In: Proceedings of the 16th Symposium (International) on Combustion, pp. 605–617.
Le Clercq, P., Bellan, J., 2002. Direct numerical simulation of a temporal mixing layer laden with multicomponent evaporating droplets. AIAA Paper 2002-0338.
Martin, J.E., Meiburg, E., 1994. The accumulation and dispersion of heavy particles in forced two-dimensional mixing layers. I. The fundamental and subharmonic cases. Phys. Fluids 6, 1116–1132.
Mashayek, F., 1998a. Direct numerical simulations of evaporating droplet dispersion in forced low-Mach number turbulence. Int. J. Heat Mass Transfer 41, 2601–2617.
Mashayek, F., 1998b. Droplet-turbulence interactions in low Mach number homogeneous shear two-phase flows. J. Fluid Mech. 367, 163–203.
Mashayek, F., Jaberi, F.A., 1999. Particle dispersion in forced isotropic low-Mach number turbulence. Int. J. Heat Mass Trans. 42, 2823–2836.
Mashayek, F., Jaberi, F.A., Miller, R.S., Givi, P., 1997. Dispersion and polydispersity of droplets in stationary isotropic turbulence. Int. J. Multiphase Flow 23, 337–355.
Miller, R.S., 2001. Effects of non-reacting solid particle and liquid droplet loading on an exothermic reacting mixing layer. Phys. Fluids 13, 3303–3320.
Miller, R.S., Bellan, J., 1999. Direct numerical simulation of a confined three-dimensional gas mixing layer with one evaporating hydrocarbon-droplet laden stream. J. Fluid Mech. 384, 293–338.
Miller, R.S., Bellan, J., 2000. Direct numerical simulation and subgrid analysis of a transitional droplet laden mixing layer. Phys. Fluids 12, 650–671.
Miller, R.S., Harstad, K., Bellan, J., 1998. Evaluation of equilibrium and non-equilibrium evaporation models for many-droplet gas–liquid flow simulations. Int. J. Multiphase Flow 24, 1025–1055.
Moser, R.D., Rogers, M.M., 1991. Mixing transition and the cascade to small scales in a plane mixing layer. Phys. Fluids A 3, 1128–1134.
Okong'o, N., Bellan, J., 2000. A priori subgrid analysis of temporal mixing layers with evaporating droplets. Phys. Fluids 12, 1573–1591.
Papamoschou, D., Roshko, A., 1988. The compressible turbulent mixing layer: an experimental study. J. Fluid Mech. 197, 453–477.
Presser, C., Gupta, A.K., Avedisian, C.T., Semerjian, H.G., 1992. Combustion of methanol and methanol/dodecanol spray flames. J. Propulsion Power 8, 553–559.
Randolph, A.L., Makino, A., Law, C.K., 1986. Liquid-phase diffusional resistance in multicomponent droplet gasification. In: Proceedings of the 21st Symposium (International) on Combustion, pp. 601–608.
Samimy, M., Lele, S.K., 1991. Motion of particles with inertia in a compressible free shear layer. Phys. Fluids 3, 1915–1923.
Sandham, N., Reynolds, W., 1989. The compressible mixing layer: linear theory and direct simulations. AIAA Paper 89-0371.

Sangiovanni, J.J., Kesten, A.S., 1976. Effects of droplet interaction on ignition in monodispersed droplet streams. Proc. Combust. Inst. 16, 577–592.

Sirignano, W.A., 1993. Fluid dynamics of sprays. J. Fluids Eng. 115, 345–378.

Sirignano, W.A., 1999. Fluid Dynamics and Transport of Droplets and Sprays. Cambridge University Press, New York, New York.

Sirignano, A., Law, C.K., 1978. Transient heating and liquid phase mass diffusion in droplet vaporization. Adv. Chem. Ser. 166, 1–26.

Spalding, D.B., 1953. Experiments on the burning and extinction of liquid fuel spheres. Fuel 32, 169–185.

Varanasi, K. 2001. Direct numerical simulation of a multicomponent droplet laden mixing layer. Masters thesis. Clemson University, Department of Mechanical Engineering.

Wood, B.J., Wise, H., Inami, S.H., 1960. Heterogenous combustion of multicomponent fuels. Combust. Flame 4, 235–242.